Journal of Plant Physiology 171 (2014) 97–108

Contents lists available at ScienceDirect

Journal of Plant Physiology

journal homepage: www.elsevier.com/locate/jplph

Physiology

Organization of perinuclear actin in live tobacco cells observed by PALM with optical sectioning

Steffen Durst[a], Per Niklas Hedde[b], Linda Brochhausen[a], Peter Nick[a], Gerd Ulrich Nienhaus[b,c], Jan Maisch[a,*]

[a] Botanical Institute, Molecular Cell Biology, Karlsruhe Institute of Technology (KIT), Kaiserstraße 2, D-76131 Karlsruhe, Germany
[b] Institute of Applied Physics and Center for Functional Nanostructures (CFN), Karlsruhe Institute of Technology (KIT), Wolfgang-Gaede-Straße 1, D-76131 Karlsruhe, Germany
[c] Department of Physics, University of Illinois at Urbana-Champaign, Urbana, IL, USA

ARTICLE INFO

Article history:
Received 12 September 2013
Accepted 20 October 2013

Keywords:
Actin filaments
Lifeact
Nuclear migration
Photoactivatable fluorescent proteins
Photoactivated localization microscopy

ABSTRACT

Actin performs a wide variety of different tasks. This functional diversity may be accomplished either by the formation of different isotypes or by suitable protein decoration that regulates structure and dynamics of actin filaments. To probe for such a potential differential decoration, the actin-binding peptide Lifeact was fused to different photoactivatable fluorescent proteins. These fusions were stably expressed in *Nicotiana tabacum* L. cv. Bright Yellow 2 cells to follow dynamic reorganization of the actin cytoskeleton during the cell cycle. The Lifeact–monomeric variant of IrisFP fusion protein was observed to indiscriminately label both, central and cortical, actin filaments, whereas the tetrameric Lifeact–photoswitchable red fluorescent protein fusion construct selectively labeled only a specific perinuclear sub-population of actin. By using photoactivated localization microscopy, we acquired super-resolution images with optical sectioning to obtain a 3D model of perinuclear actin. This novel approach revealed that the perinuclear actin basket wraps around the nuclear envelope in a lamellar fashion and repartitions toward the leading edge of the migrating nucleus. Based on these data, we suggest that actin that forms the perinuclear basket differs from other actin assemblies by a reduced decoration with actin binding proteins, which is consistent with the differential decoration model.

Introduction

Plant actin has to fulfill a great variety of different tasks. It is essential for intracellular transport of various cargoes such as organelles including peroxisomes (Mathur et al., 2002), chloroplasts (Kadota et al., 2009), mitochondria (Van Gestel et al., 2002), and Golgi vesicles (Boevink et al., 1998). Most of these transport events are accomplished by myosin motors (Shimmen and Yokota, 2004; Shimmen, 2007; Ueda et al., 2010). Actin filaments (AFs) structure the vacuolar and transvacuolar cytoplasmic strands of plant cells (Staiger et al., 1994; Verbelen and Tao, 1998; Sheahan et al., 2007). Furthermore, the actin cytoskeleton is responsible for anchoring organelles at defined intracellular positions (Frey et al., 2010; Klotz and Nick, 2012), and supports the integrity of the plasma membrane (Hohenberger et al., 2011). Consequently, AF strongly control the entire cellular architecture. In order to perform all these different tasks, the actin cytoskeleton has to reorganize between different arrays that also differ in their dynamics. For example, the control of nuclear position during the cell cycle requires stable actin cables, whereas the filaments located in the cortical regions of a cell, where they mediate the immediate responses to external stimuli such as pathogens (Qiao et al., 2010) or auxin flux (for review, see Nick, 2010), have to be highly dynamic. Plants probably use actin as a sensor to monitor stress or developmental signals by alterations of the polymerization status, which in turn can be used to trigger apoptosis/programmed cell death (for review, see Franklin-Tong and Gourlay, 2008; Smertenko and Franklin-Tong, 2011). The coexistence of different actin arrays within the same cell raises the question as to how functional diversity is regulated on the molecular level. Two general concepts are proposed; either different filament arrays are composed of different isotypes, or AF are differentially decorated by diverse accessory proteins defining structure and dynamics. It should be noted that both mechanisms are not mutually exclusive.

In support of the actin-binding protein (ABP) model, we note that plant actins share 83–88% amino acid sequence identity with

Abbreviations: ABP, actin-binding protein; AFs, actin filaments; BY-2, *Nicotiana tabacum* L. cv. Bright Yellow 2 cell culture; mIrisFP, monomeric variant of IrisFP; pa-FP, photoactivatable fluorescent protein; PALM, photoactivated localization microscopy; psRFP, photoswitchable red fluorescent protein.

* Corresponding author. Tel.: +49 721 608 42993; fax: +49 721 608 44193.
E-mail address: Jan.Maisch@kit.edu (J. Maisch).

0176-1617/$ – see front matter © 2013 Elsevier GmbH. All rights reserved.
http://dx.doi.org/10.1016/j.jplph.2013.10.007

actins of green algae, most protists, fungi, and animals. Within a given kingdom, the amino acid sequence identity is even higher, reaching up to 95% (Meagher et al., 1999a,b). Therefore, actin is extremely conserved. Despite this conservation, there is evidence of isovariant dynamics as a mechanism defining different functionalities; although mutations in specific actin genes produced relatively mild phenotypes in *Arabidopsis thaliana*, there were severe defects when two isotypes were inactivated (Kandasamy et al., 2009). Moreover, some of these defects (for instance impaired elongation of root hairs) revealed specificities in isovariant function. On the other hand, some of these actin isotypes, when expressed under the control of multiple regulatory sequences, were able to completely rescue normal development in the absence of other isotypes indicating a certain degree of functional redundancy.

As an alternative to isovariant dynamics, functional diversity could be regulated by the huge variety of ABPs. These proteins control the assembly of monomeric actin into filamentous actin (F-actin), the maintenance of F-actin, as well as its disassembly and organization, such as bundling or branching (Hussey et al., 2002; Staiger and Blanchoin, 2006; for review, see Staiger et al., 2010). It might be the specific decoration of AF with ABPs that leads to multiple functional subpopulations, and allows them to perform the different tasks mentioned above. Over the last decades, fluorescence microscopy has proven to be a powerful technique to address cell biological questions. To detect different levels of actin decoration, fluorescent probes specifically binding to distinct actin subpopulations depending on the degree of steric hindrance could be used. However, conventional optical microscopy using visible light is restricted to ~200 nm in resolution due to Abbe's law. In recent years, super-resolution microscopy techniques such as photoactivated localization microscopy (PALM, Betzig et al., 2006), or stochastic optical reconstruction microscopy (STORM, Rust et al., 2006) have attracted considerable attention because they allow structures below the Abbe limit to be resolved (for review, see Hedde and Nienhaus, 2010). To visualize AF in living, walled plant cells with super-resolution, we have applied PALM, which is based on the localization of individual fluorophores. It requires labeling with fluorophores that can be stochastically activated to their fluorescent form by light irradiation. Thus, we have fused photoactivatable fluorescent proteins (pa-FPs) to the actin-binding probe Lifeact. In their native forms, fluorescent proteins are often found to form tetramers (Wiedenmann and Nienhaus, 2006). Tetrameric pa-FPs carry four fluorophores and thus have the advantage of yielding a strong fluorescence signal. Therefore, they are well suited for labeling whole cells and organelles. In applications involving a fusion partner, however, their large size and tetrameric nature might interfere with the proper localization and function of their fusion partner. Consequently, many of these FPs have been engineered into monomeric variants (Nienhaus et al., 2006). Monomeric pa-FPs are valuable tools for labeling and tracking individual molecules inside a cell (for review, see Lukyanov et al., 2005).

Here we have used the photoswitchable red fluorescent protein (psRFP; Fuchs, 2011) for visualization of AFs. This tetrameric protein shows reversible photoswitching between a non-fluorescent and a fluorescent state. In addition, we have employed the monomeric variant of IrisFP (mIrisFP; Fuchs et al., 2010), which combines photoconversion with reversible photoswitching. Both proteins were C-terminally fused to Lifeact, a valuable actin-binding probe reported to have the fewest side effects (Riedl et al., 2008) when correct expression levels of Lifeact have been determined (Van der Honing et al., 2011). These fusions were stably expressed in tobacco BY-2 cells to follow organization, polarity and dynamics of the actin cytoskeleton. Here, we show that differentially decorated and, therefore, functionally distinct AF-sub-populations can be distinguished by choosing either monomeric or the much larger tetrameric Lifeact–FP fusions. This interesting and extremely useful property presumably derives from steric hindrance of the tetrameric psRFP reporter upon binding to AFs that are heavily decorated with ABPs. In addition to standard fluorescence microscopy for visualization and discrimination of diversely decorated AF sub-populations *in vivo*, we have also employed PALM with optical sectioning to obtain three-dimensional images of live plant cells.

Materials and methods

Tobacco cell cultures

BY-2 (*Nicotiana tabacum* L. cv. Bright Yellow 2) suspension cell lines (Nagata et al., 1992) were cultivated as described in Maisch and Nick (2007). Transgenic cells and calli were supplemented with 50 mg L^{-1} hygromycin. For phenotyping experiments, the cell lines were assessed in the absence of selective pressure to exclude possible side effects without any detectable differences in patterning, MI, cell length, cell width or arrangement of AF.

Cloning procedure

Plasmids for stable and transient transformation of BY-2 WT cells were constructed using the Gateway® cloning technology (Invitrogen Corporation, Paisley, UK). The sequences encoding Lifeact–photoswitchable red fluorescent protein (psRFP) and Lifeact–monomeric variant of IrisFP (mIrisFP) (Supplementary Data S8) were amplified by PCR using oligonucleotide primers with Gateway®-specific flanks (**attB1-Lifeact–pa-FP**: 5′-GGGG **ACA AGT TTG TAC AAA AAA GCA GGC TTC** ATG GGA GTA GCA GAT CTA ATC-3′; **attB2-Lifeact–mIrisFP**: 5′-GGGG **AC CAC TTT GTA CAA GAA AGC TGG GTC** TTA TCG TCT GGC ATT GTC AG-3′; **attB2-Lifeact–psRFP**: 5′-GGGG **AC CAC TTT GTA CAA GAA AGC TGG GTC** TTA GTG ATG TCC AAG CTT GG-3′). As template pcDNA3 vectors (Invitrogen Corporation, Paisley, UK) containing the sequences of Lifeact–psRFP and Lifeact–mIrisFP were used, respectively. The resulting gene regions were inserted into the binary vector pH7WG2 (Karimi et al., 2002) following the manufacturer's protocol (Invitrogen Corporation, Paisley, UK). To confirm the accuracy of the sequences, both fusion constructs were verified by restriction digest and sequencing (GATC, Konstanz, Germany).

Transient and stable expression

Biolistic transformation was performed as described in Maisch et al. (2009). Following bombardment, the cells were incubated for 4–24 h in the dark at 26 °C, and observed under the fluorescence microscope.

Stable transformation of non-transformed BY-2 WT cells with the binary vector constructs pH7WG2–Lifeact–psRFP and pH7WG2–Lifeact–mIrisFP was achieved according to Buschmann et al. (2011). Both constructs were transformed into *Agrobacterium tumefaciens* (strain LBA 4404; Invitrogen Corporation, Paisley, UK) via heatshock (5 min, 37 °C). The transformed cells were cultivated on plates containing MS agar and 100 mg L^{-1} cefotaxime and 50 mg L^{-1} hygromycin driving selection pressure.

Visualization of AF by phalloidin-based staining

AFs were visualized by the method of Kakimoto and Shibaoka (1987) modified according to Olyslaegers and Verbelen (1998), as described in Maisch et al. (2009).

Determination of frequency distribution, cell length and width

Division synchrony of tobacco BY-2 cells was quantified by collecting 0.5-mL aliquots of cells 4 days after inoculation and immediate observation under an AxioImager Z.1 microscope (Zeiss, Jena, Germany). Differential interference contrast images were obtained by a digital imaging system (AxioVision; Zeiss). Frequency distributions over the number of cells per individual file were constructed as described in Maisch and Nick (2007). Each data point represents 1200 cell files from at least three independent experimental series. Cell length and width were also determined from the central section of the cells according to Maisch and Nick (2007). Each data point represents mean and standard error from 500 individual cells from four independent experimental series.

Determination of mitotic index

The mitotic index (MI) of tobacco BY-2 cell suspensions was determined as described in Maisch and Nick (2007). Mitotic indices were determined as the relative frequency of mitotic cells out of a sample of 500 cells scored for each data point.

Nuclear positioning

Nuclear positions (NP) in tobacco BY-2 were assessed 1 day after subcultivation from DIC images of central sections of the cells using the length measurement function of the AxioVision software (Zeiss, Jena, Germany). NP were determined as relative values by division of the shortest distance between the middle of the nucleus and the total cell diameter (Frey et al., 2010). Typical values for mean NP were clustered into three main intervals indexed by the attributes lateral (NP = 0.15–0.28), intermediate (NP = 0.3–0.4), and central (NP = 0.4–0.5). For each time point and cell line, four times 500 cells were measured, mean values, SE, and occurrence distributions calculated.

Microscopy and image analysis

For morphological studies, cells were examined under an AxioImager Z.1 microscope (Zeiss, Jena, Germany) equipped with an ApoTome microscope slider for optical sectioning and a cooled digital CCD camera (AxioCam MRm; Zeiss). (ps)RFP-, mIrisFP-/Alexa-Fluor® 488-fluorescence were observed through the filter sets 43 HE (excitation: 550 nm, beamsplitter: 570 nm, emission: 605 nm) and 38 HE (excitation: 470 nm, beamsplitter: 495 nm, emission: 525 nm), respectively (Zeiss). Activation of psRFP-fluorescence was performed with 550-nm light. Stacks of optical sections were acquired at different step sizes between 0.4 and 0.8 μm. Images were processed and analyzed using the AxioVision (Rel. 4.8.2) software.

For the analysis of the division pattern, cells were imaged with the same microscope using a 20× objective and differential interference contrast illumination. For presentation, the images were post-processed with respect to contrast and brightness using ImageJ (NIH, Bethesda, USA).

For photoactivation localization microscopy (PALM) of Lifeact–psRFP ox BY-2 cells, 0.5 mL cells at various days after subcultivation were transferred from their standard cultivation flasks into Chamber SlidesTM (4 chambers, Thermo Scientific, Langenselbold, Germany) and observed using a widefield microscope setup of our own design. It is based on a modified Axio Observer.Z1m (Zeiss, Jena, Germany) equipped with a 63×/1.46 oil immersion objective. The internal stepper motor was used for optical sectioning in 2 μm steps. Movement was performed after acquisition of 3000 frames for each section. The photostability of psRFP allowed a total of 6–9 sections (18,000–27,000 frames) per stack to be collected. Excitation and on-switching of Lifeact–psRFP was performed using 561-nm light (GCL-150-561, CrystaLaser, Reno, NV) at intensities of 50–200 W/cm^2. For PALM imaging, sparse photoactivation of the marker is necessary to ensure that individual molecules are spatially sufficiently separated for subsequent localization. psRFP has identical photoactivation and excitation wavelengths. Thus, especially at the start of imaging, the density of activated markers can be too high. Therefore, off-switching was induced by using 473-nm light (LSR473-200-T00, Laserlight, Berlin, Germany) at <10 W/cm^2. Intensities were adjusted using an Acousto Optic Tunable Filter (AOTFnC-400.650, A-A, Opto-Electronic, Orsay Cedex, France). Fluorescence light was filtered using a 610/75 nm bandpass (Chroma HQ610/75, AHF, Tübingen, Deutschland) and detected by an EMCCD camera (iXon897, Andor, Belfast, Ireland) set to an exposure time of 30–50 ms. We reconstructed the PALM images using our own software (Hedde et al., 2009) written in Matlab R2009b (The MathWorks, Natick, MA).

Latrunculin B treatment

Latrunculin B from *Latrunculia magnifica* (Sigma–Aldrich) was added directly to the final concentration of 50, 100, and 200 nM into the standard culture medium using a filter-sterilized stock of 1 mM Latrunculin B dissolved in 96% (v/v) ethanol.

Preparation of tobacco BY-2 protoplasts

For preparation of tobacco BY-2 protoplasts, 4 mL of Lifeact–psRFP ox cells and GFP-FABD2 cells (Maisch et al., 2009) were taken 3 days after subcultivation according to Kuss-Wymer and Cyr (1992) and Wymer et al. (1996).

Regeneration of walled BY-2 suspension cells was performed as described in Zaban et al. (2013). Hygromycin in a final concentration of 30 mg L^{-1} was added to all used solutions. Observation of the protoplasted Lifeact–psRFP ox BY-2 cells started immediately after the transfer into regeneration solution and was repeated every 24 h up to 3 days.

Results

Lifeact–psRFP localizes only at actin structures forming the nuclear basket

In the stably transformed, Lifeact–psRFP overexpressing BY-2 tobacco cell line fluorescence could be detected exclusively from around the nucleus. The cells did not exhibit a single red fluorescent filamentous structure in the cell cortex or in transvacuolar strands. Only a tight filamentous, basket-like structure around the nucleus was labeled by the tetrameric probe (Fig. 1a and b).

To test why only the perinuclear actin was manifested in the stably transformed Lifeact–psRFP BY-2 cells, these cells were PFA-fixed and stained using Alexa-Fluor® 488 labeled phalloidin three days after subcultivation. This approach allowed visualization of other actin sub-populations beyond those of the nuclear basket that were not marked via Lifeact–psRFP expression. For the nuclear basket, a clear colocalization of green Alexa-Fluor® 488 (Fig. 1c) and red Lifeact–psRFP (Fig. 1d) could be detected, resulting in a yellow signal in the merged image (Fig. 1e). This observation shows that actin is indeed labeled by Lifeact–psRFP. However, in the cell cortex, solely the green fluorescence of Alexa-Fluor® 488 phalloidin could be detected, whereas the red Lifeact–psRFP signal was completely absent (Fig. 1c–e), indicating that there is a clear structural difference between these actin sub-populations.

Interestingly, a small sub-population of Lifeact–psRFP overexpressing cells displayed a fully decorated actin cytoskeleton

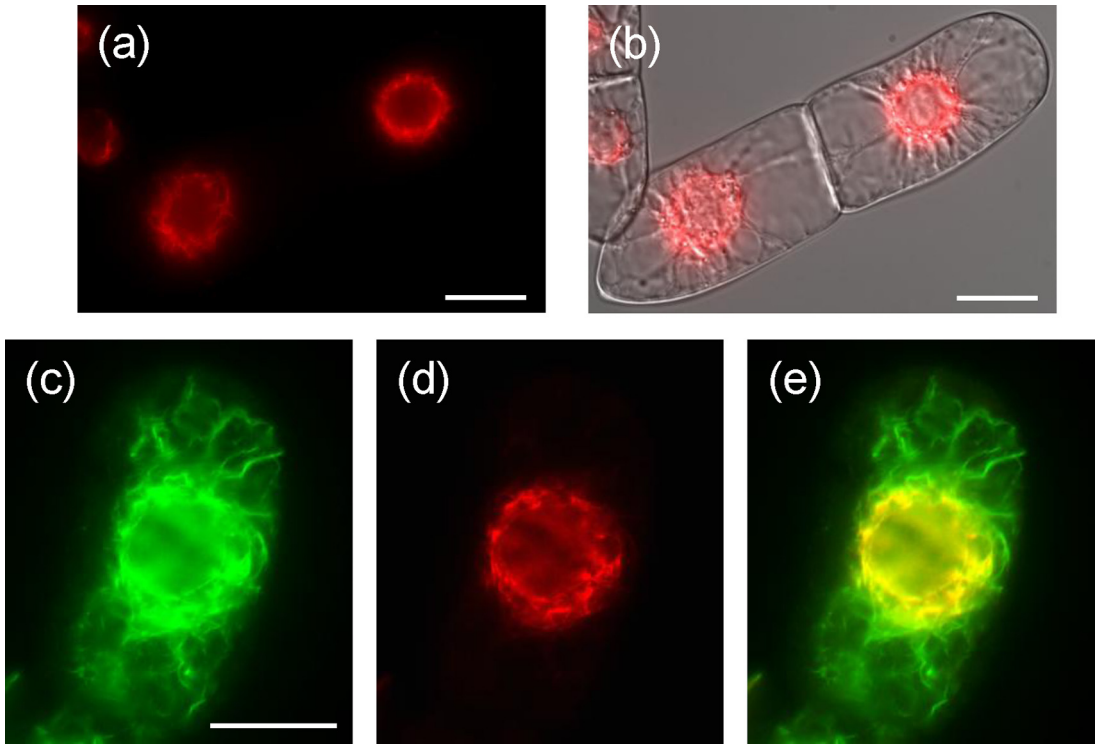

Fig. 1. Visualization of AFs in Lifeact–psRFP ox BY-2 cells by stably expressed Lifeact–psRFP and AlexaFluor® 488 phalloidin. (a) Lifeact–psRFP ox BY-2 cell *in vivo*, red channel: Lifeact–psRFP and (b) merge of red channel and DIC. (c)–(e) Whole Lifeact–psRFP ox BY-2 cell; green channel: AlexaFluor® 488 phalloidin (c); red channel: Lifeact–psRFP (d); (e) merge of (c) and (d), yellow signal marks colocalization. Scale bars: 20 μm. (For interpretation of the references to color in this figure legend, the reader is referred to the web version of the article.)

comprising both central and cortical arrays (Supplementary Data S1). Those cells were apparently undergoing cell death, as indicated by an almost complete cessation of cytoplasmic streaming, membrane detachment and deformation in cell shape. In addition to the stably transformed Lifeact–psRFP ox BY-2 cell line, a biolistic transient transformation was performed. Numerous cells expressing Lifeact–psRFP could be detected 24 h after transient transformation. The intracellular localization pattern was nearly identical with the pattern of a Lifeact–mIrisFP construct. Both constructs marked highly specific and distinctive structures with characteristic properties of AFs such as Y-crossings and cortical arrangements. The Lifeact–mIrisFP construct contained the identical vector backbone and Lifeact sequence as the Lifeact–psRFP construct and was used as a control for the localization of the Lifeact–FP fusions in transiently as well as stably transformed BY-2 cells (Supplementary Data S2).

Lifeact–psRFP localization during mitosis

To assess possible changes in the localization of the Lifeact–psRFP signal, we have followed mitosis of stably transformed BY-2 cells over time. As observed before, the Lifeact–psRFP signal was exclusively localized around the nucleus during mitosis, and the nuclear basket of Lifeact–psRFP-labeled AF was observed to be quite stable. Until the end of metaphase, the whole structure was contiguous. The filaments were arranged in a fine mesh-like conformation (Fig. 2b and c). Starting with anaphase, the AF of the basket became more bundled and a slight gradient of the Lifeact–psRFP signal appeared (Fig. 2d). Especially during the later mitotic phases, a clear increase of signal intensity toward the cell poles was detected (Fig. 2d and e). Upon completion of mitosis and cytokinesis, the new nuclei migrated to the center of both daughter cells and were completely coated by Lifeact–psRFP marked nuclear baskets (Fig. 2f). It should be noted that, throughout mitosis, the basket visualized by Lifeact–psRFP remained outside the spindle proper.

Lifeact–psRFP localization during cell cycle

Intracellular localization and signal intensity of the fusion protein persisted through the whole cell cycle in stably transformed Lifeact–psRFP ox cells. Nevertheless, the localization pattern around the nuclear envelope shifted sometimes and formed a gradient. Three main types of patterns could be distinguished. The most frequent one was a relatively homogenous distribution around the whole nucleus. Sometimes, a clear gradient toward the nearest cell wall appeared (which in most cases is the wall that had been deposited most recently) and, lastly, a gradient toward the cell center was found at a comparable frequency. These gradients of the Lifeact–psRFP signal were near the leading edge and correlated with nuclear migration characteristic of the cell cycle in vacuolated plant cells (Fig. 3).

In Lifeact–psRFP ox BY-2 cells passing through the late G1-phase, the psRFP signal was mainly localized between the nucleus and the lateral cell wall (Fig. 3a). During migration of the nucleus toward the cell center, Lifeact–psRFP emission was always strongest at the side of the nucleus adjacent to the cell center (Fig. 3b). Cells, for which the nucleus had reached this position essentially lost the Lifeact–psRFP gradient, and the signal became distributed like a nuclear basket (Fig. 3c). This conformation was relatively stable until the end of mitosis. In anaphase, the psRFP fluorescence was exclusively localized at the poles of the former nucleus (Fig. 3d). However, at the end of mitosis, in late telophase, the whole Lifeact–psRFP emission shifted in-between the new cell wall and the nuclei (Fig. 3e). Following this stage of the cell cycle, a

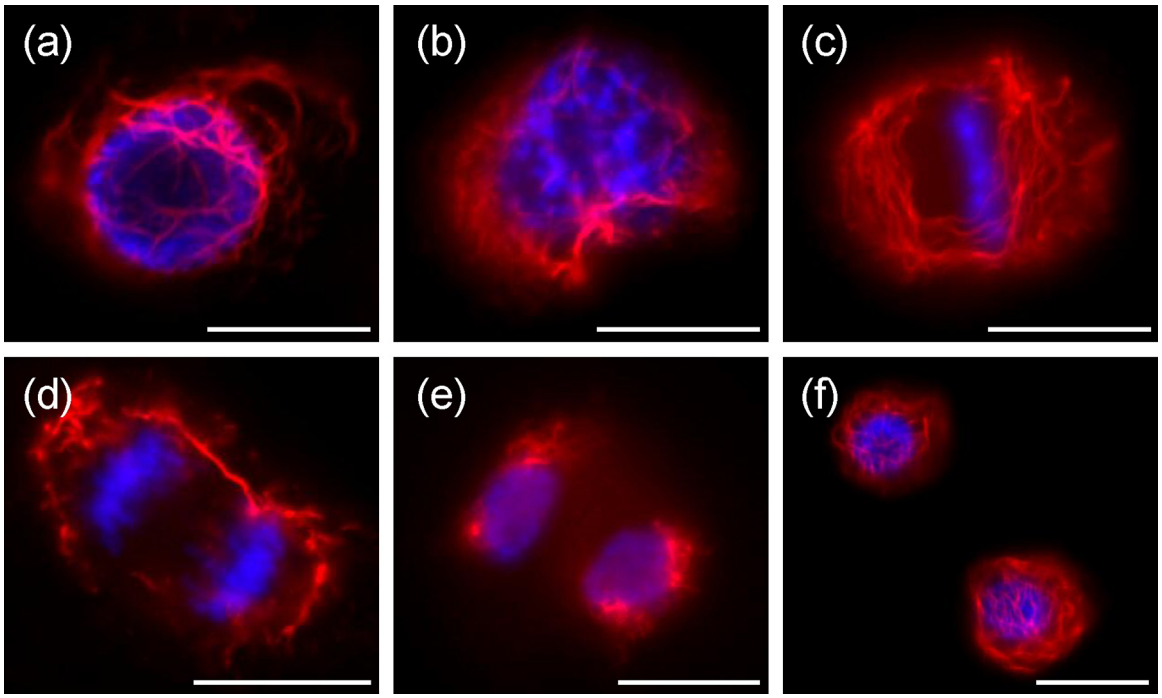

Fig. 2. Representative images of different phases of mitosis in Lifeact–psRFP ox BY-2 cells. (a) Interphase. (b) Prophase; chromosomes already condensed; fine filamentous nuclear basket intact. (c) Metaphase; chromosomes arranged in the equatorial plane; nuclear basket consists of very fine Lifeact–psRFP marked AF. (d) Anaphase; chromosomes are pulled to the cell poles; nuclear basket reduced to slightly bundeled filaments with moderate gradient toward cell poles. (e) Telophase; new nuclear envelop has been formed and the nucleus becomes round again; clear gradient of the Lifeact–psRFP marked AF toward the cell poles. (f) Two daughter cells short after finished mitosis; nuclei already in the center of the cells; very homogenous nuclear actin basket. Lifeact–psRFP signal: red; Hoechst 33528 stained DNA: blue. Scale bars: 20 μm. (For interpretation of the references to color in this figure legend, the reader is referred to the web version of the article.)

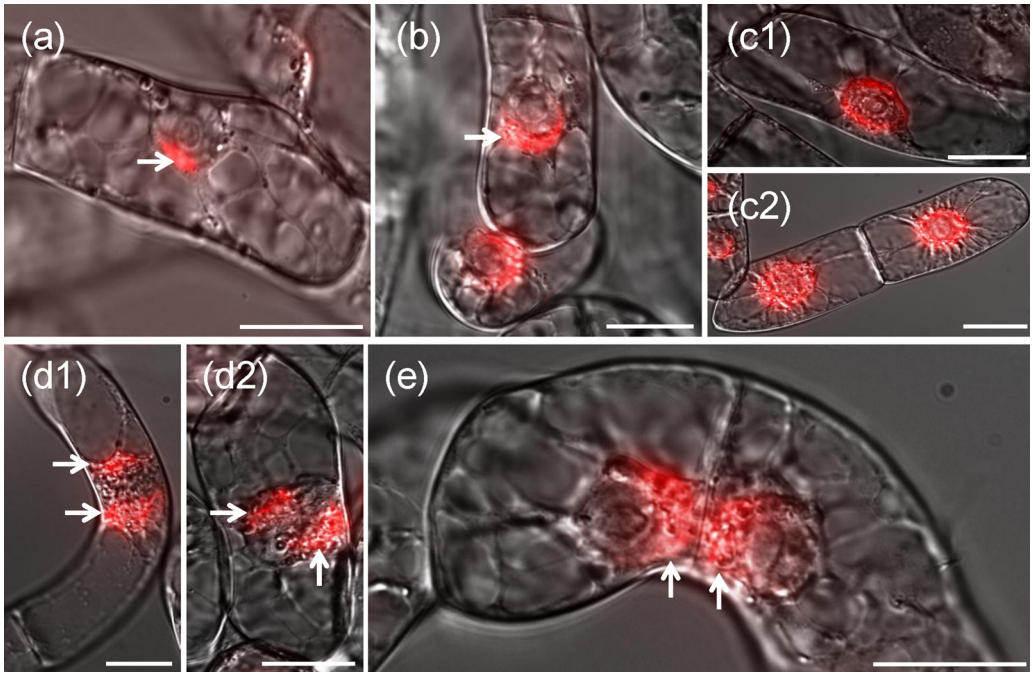

Fig. 3. Representative images of Lifeact–psRFP ox BY-2 cells during cell cycle. (a) Interphase cell; nucleus is attached to the lateral cell wall, Lifeact–psRFP signal between cell wall and nucleus. (b) Interphase cell; nucleus is moving into the center of the cell and prepares for mitosis; Lifeact-RFP signal is oriented toward the cell center. (c1) Interphase cell; nucleus reached cell center; Lifeact–psRFP signal labels whole nuclear basket. (c2) Start of mitosis; nuclei of both cells in prophase; very fine filaments of nuclear basket homogenously marked by Lifeact–psRFP signal. (d1) Mitotic cell in anaphase; Lifeact–psRFP signal at both poles of the former nucleus. (d2) Cell with abnormal position of division plane leading to insertion of a non-perpendicular new cross wall. (e) End of mitosis; new cell wall has been formed; Lifeact–psRFP signal exclusivly between new cell wall and nuclei. White arrows indicate peaks of Lifeact–psRFP signal gradient. Scale bars: 20 μm.

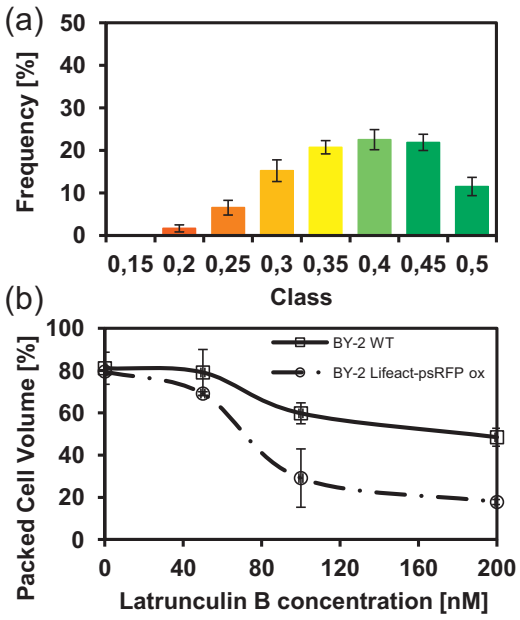

Fig. 4. Nuclear positioning and Latrunculin B sensitivity of Lifeact–psRFP ox BY-2 cells. (a) Influence of Lifeact–psRFP expression on nuclear positioning. Data acquisition and categorization according to Frey et al. (2010). Three main intervals for the position of the nucleus in a cell of interest can be defined, indicating either a central location of the nucleus (NP = 0.4–0.5; shaded in green), a lateral position (NP = 0.15–0.28, shaded in red), or an intermediate state (NP = 0.3–0.4, shaded in bright yellow). (b) Latrunculin B treatment of non-transformed BY-2 WT (open boxes, continous curve) and Lifeact–psRFP ox (open circles, long-dash-dotted curve) cells. Values represent relative cell volume of 15 mL liquid cell culture. All experimental data are derived from three independent experimental series; error bars = SE. (For interpretation of the references to color in this figure legend, the reader is referred to the web version of the article.)

rotation of the whole nuclei, but not a reorientation of AFs around the nuclei could be observed, reorienting the Lifeact–psRFP gradients in the direction of the new cell centers (Supplementary Data S3).

Phenotyping of Lifeact–psRFP ox BY-2 cells

To test for effects of the transgene expression, parameters such as the ratio of length and width, mitotic index, cell viability, nuclear positioning, and division pattern were analyzed. Lifeact–psRFP ox BY-2 cells were slightly longer than cells of the non-transformed WT control, showed a marginally reduced mitotic index, possessed a comparable cell viability, and their division pattern was nearly identical to the control cell line (Maisch and Nick, 2007). In contrast to these parameters, the nuclear positioning in the transgenic cell line differed from the control. At day 1 after subcultivation, nearly 50% of the cell nuclei of non-transformed BY-2 WT control cells were located in the cell center for mitosis and cytokinesis (Frey et al., 2010). In Lifeact–psRFP ox BY-2 cells, only about 10% of the nuclei were in the cell center at this time, and nuclear migration was clearly delayed (Fig. 4a).

In contrast to Lifeact–mIrisFP, the Lifeact–psRFP fusion protein forms tetramers, such that one protein complex harbors four Lifeact peptides for actin-binding. This could introduce cross-linking of the actin around the nucleus, where the microfilament meshwork is very dense in comparison to the cortical region. Cross-linked AFs would be stabilized and less sensitive to cytoskeletal drugs such as Latrunculin B. Therefore, the sensitivity of the Lifeact–psRFP ox cell line was compared to a non-transformed BY-2 WT cell culture by constructing a dose–response curve of packed cell volume as a measure of culture growth over the concentration of Latrunculin B (LatB). As Fig. 4b shows, the Lifeact–psRFP ox cell line is not less but more sensitive to LatB as compared to the non-transformed WT BY-2 cells. Both lines were treated with LatB in different concentrations (50, 100, and 200 nM), incubated for 4 days, and evaluated after further 24 h of settling down at 4 °C. At a final concentration between 60 and 80 nM LatB, the Lifeact–psRFP ox cell volume was already reduced to 50% compared to the untreated Lifeact–psRFP ox cells, whereas the non-transformed BY-2 WT cell volume was only diminished by 5–10% in relation to the control.

PALM shows the leading edge of nuclear movement in 3D

Images of stably transformed Lifeact–psRFP ox BY-2 cells recorded by confocal laser scanning and epifluorescence microscopy always showed a nuclear basket of actin without any signal in the cortical or transvacuolar cell regions. This observation raised the question as to why the fusion protein can only be observed around the nucleus. Also, based on the standard microcopy images, it is not entirely clear if the actin arrangement around the nucleus is still composed of filaments and how these are arranged. Therefore, in addition to conventional fluorescence microscopy, we visualized AFs within living tobacco BY-2 cells in more detail by application of super-resolution PALM, using Lifeact–psRFP as a photoswitchable marker. With this probe, we succeeded in PALM imaging of multiple layers within the sample, so that we obtained a 3D stack of the entire nuclear basket with high lateral resolution (35 ± 18 nm localization precision). To this end, we acquired and processed 27,000 images of nine sections (3000 frames each, with an axial separation of 2 μm), so that an entire BY-2 nucleus and its nuclear actin basket could be visualized in 3D. Details of the imaging procedure are described in the methods section. Fig. 5 displays the reconstructed PALM image projection (Fig. 5a), the full projection of the widefield acquisition (Fig. 5b) as well as the PALM images of the individual sections (Fig. 5c and Supplementary Data S4). The rendered 3D-structure is shown in Supplementary Data S5. As with widefield fluorescence microscopy (Fig. 1), only actin around the nucleus was visible via single-molecule localization of Lifeact–psRFP fusion proteins. We also note that no fluorescence was detected from within the nucleus as well as from other regions of the cell not adjacent to the nucleus. The filamentous nature of the perinuclear actin basket is clearly visible in the PALM images. The dual labeling of the perinuclear cage visualized by the psRFP-marker and a general actin stain using fluorescent phalloidin (Fig. 1) showed actin cables emanating from the nucleus in a radial fashion, so the AFs are oriented perpendicular to the surface of the nuclear envelope. The super-resolution images, however, clearly reveal a network of AFs enclosing the nucleus in a lamellar fashion, *i.e.*, with AFs oriented parallel to the surface of the nuclear envelope (also see Supplementary Data S6). In addition, we were able to visualize the asymmetry of the perinuclear actin basket (Fig. 6) during nuclear migration in much greater detail as compared to standard widefield fluorescence microscopy (Fig. 3). In this case, 18,000 images of six sections (3000 frames each, with an axial separation of 2 μm) were acquired and processed. The clear gradient of the Lifeact–psRFP signal is obvious; throughout all sections, the Lifeact–psRFP signal is oriented toward one particular side of the nucleus (Fig. 6c). A closer look on the individual images of the stack shows that the innermost AF oriented parallel to the leading edge of the moving nucleus are more bundled compared to the remaining AF.

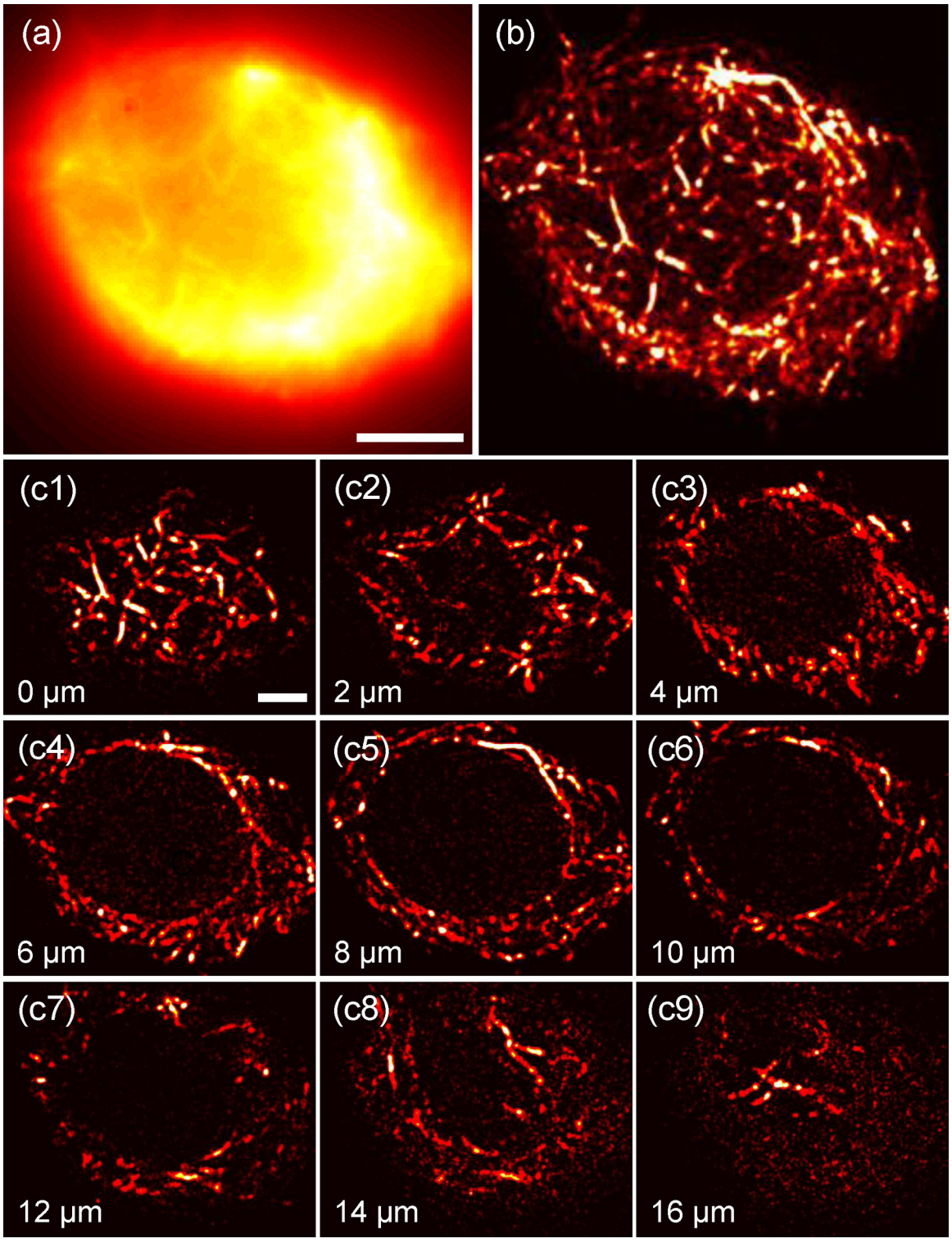

Fig. 5. PALM analysis of Lifeact–psRFP ox BY-2 cells. (a) Widefield image of a nuclear actin basket representing the sum of 27,000 single images of nine sections (3000 frames each) acquired with 2 µm spacings. Scale bar: 5 µm. (b) PALM image projection reconstructed by calculating the exact location of each individual fluorophore; fine AF are exclusively observed around the nucleus. (c) PALM images of each of the nine sections acquired, *z*-axis positions are indicated in the lower left. Scale bar: 3 µm.

Discussion

A tetrameric FP-Lifeact probe labels a specific actin sub-population

In this work, we have focused on the visualization of specific sub-populations of actin in living plant cells. We have designed an FP-based strategy to probe for potential differential decoration of AFs. The yeast peptide Lifeact, which binds to a ubiquitous motif in F-actin, was used as an actin-binding probe and fused with two different FPs. For the first construct, a tetrameric psRFP (Fuchs, 2011) was employed. Due to its large size, this fusion construct should encounter steric hindrance upon binding via the Lifeact motif to

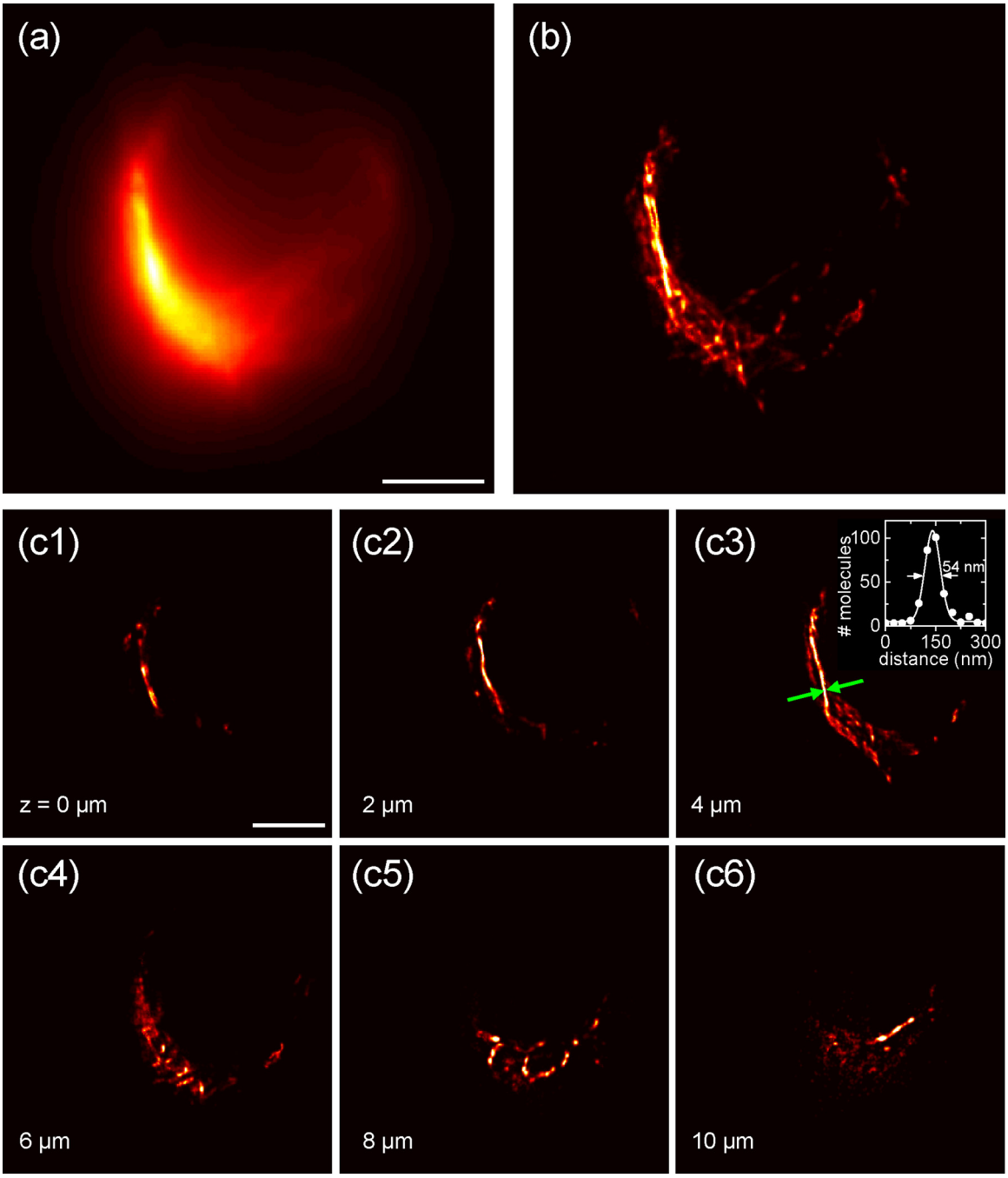

Fig. 6. PALM analysis of Lifeact–psRFP signal gradient of the nuclear basket in Lifeact–psRFP ox BY-2 cells. (a) Widefield image of a nuclear actin basket. (b) Projection of 18,000 single images of six sections (3000 frames each) with a *z*-axis distance of 2 µm; fine AF are found only near the nucleus with a clear orientation toward the direction of nuclear migration. (c) Individual sections; in panel (c3), the inset shows a cross section through an actin filament as indicated by the arrows, yielding a width of 54 nm (full width at half maximum). Scale bars: 5 µm.

actin in the presence of a dense decoration with ABPs. As a control, a second construct containing the monomeric mIrisFP was chosen, which is similar in size to the classical GFP and, thus, binds to AFs with much less steric hindrance. Moreover, both FPs are photoactivatable and offer the possibility of performing super-resolution PALM, a technique which, to our best knowledge, has not yet been applied to living plant cells. Indeed, this steric-hindrance approach was successful; a specific functional sub-population of AF in BY-2 cells could be selected and visualized with super-resolution PALM imaging which supports the model of differential decoration mechanism for functional actin diversity.

Localization pattern of Lifeact–psRFP

The fusion of Lifeact and psRFP was tested for functionality by transient transformation into BY-2 cells using the ballistic method of a particle gun (Supplementary Data S2). The efficiency was at a moderate level and the fluorescence signal of Lifeact–psRFP showed clear labeling of AFs. Since binding of the Lifeact peptide to F-actin was expected, the observed localization of the psRFP signal was not surprising. Without light irradiation psRFP is in its non-fluorescent state (Fuchs, 2011). Only upon photoactivation by yellow light (~560 nm), the chromophore isomerizes into its

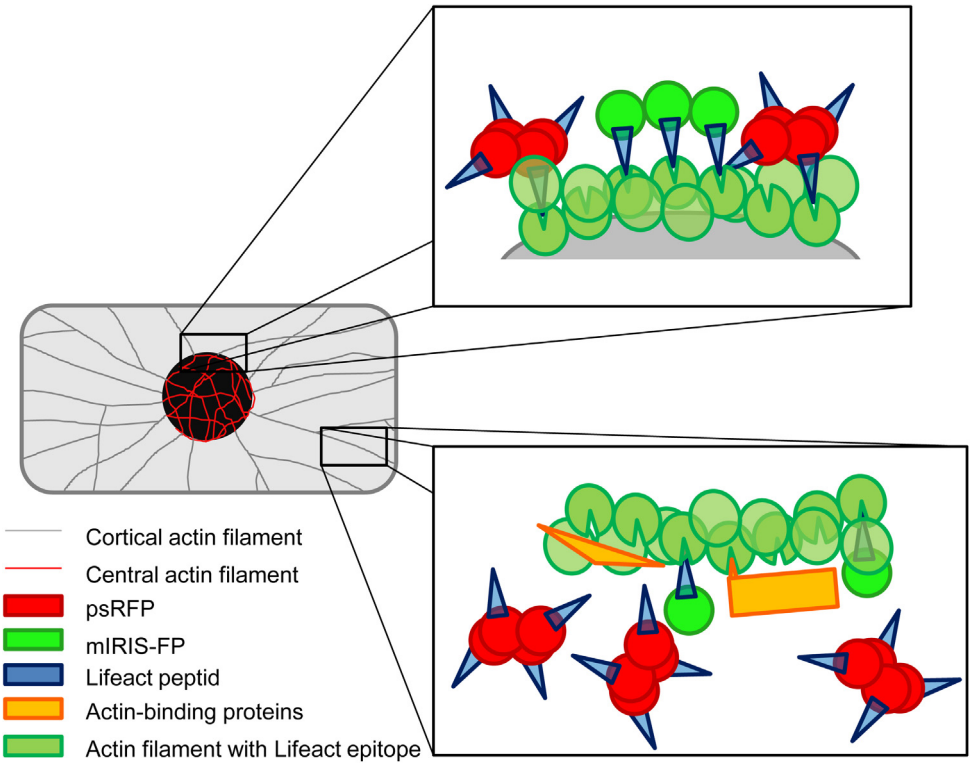

Fig. 7. Model of putative Lifeact–psRFP and Lifeact–mIrisFP binding to the nuclear actin basket and to cortical or transvacuolar AF. The Lifeact–mIrisFP construct is able to bind both sub-populations of actin, whereas the tetrameric Lifeact–psRFP is excluded at the small binding sites left freely accessible by ABP decoration. For better visibility, the FPs and especially the tiny Lifeact peptide are not depicted true to scale.

fluorescent configuration. Therefore, screened areas were first illuminated with 561 nm laser light. The AF labeled by Lifeact–psRFP as well as by Lifeact–mIrisFP were homogeneously distributed throughout the entire cell. A difference in localization could not be observed.

Since both constructs were functional, the next step was the stable transformation into BY-2 cells because the yield of transformed cells was too small to produce a sufficiently large starting population to conduct a successful PALM experiment. However, upon stable transformation, conspicuous differences emerged between the two constructs. Whereas filamentous structures were labeled throughout the entire Lifeact–mIrisFP expressing cells, similar to the transient approaches (Supplementary Data S2), only a basket-like structure around the nucleus could be detected in the Lifeact–psRFP expressing cells (Fig. 1a and b). A control with Alexa-Fluor® 488 phalloidin co-staining revealed that the structures marked by both Lifeact fusions were indeed F-actin including the basket-like structure around the nucleus (Fig. 1c–e). This observation is a strong indicator for the existence of additional sub-populations of F-actin, which are not labeled by the tetrameric fusion probe, but by Alexa-Fluor® 488 phalloidin.

As a consequence, we were able to specifically visualize different sub-populations of actin within a cell by the sole difference of the nature of the FP label (tetramer vs. monomer). The Lifeact–psRFP expressing BY-2 cells clearly revealed a difference between central and cortical AF with respect to the accessibility of the Lifeact peptide to actin. As was pointed out in the introduction, the stability and dynamics of F-actin might be controlled by ABPs and their complexes. Since actin isoforms are highly conserved, it is straightforward to assume that the decoration with different ABPs leads to the formation of functionally distinct sub-populations of actin. The sub-population constituting the nuclear basket may be accessible for the Lifeact–psRFP fusion protein because these filaments are more scarcely decorated with ABPs, whereas the cortical filaments are densely covered, thereby impeding access of the tetrameric probe (Fig. 7). Similarly, Leduc et al. (2012) showed that it is possible to generate traffic jams on microtubules by molecular crowding of kinesin-8-motor proteins.

Our model is further supported by the observation that cortical AFs in cells undergoing cell death are labeled by Lifeact–psRFP (Supplementary Data S1). Since alterations of the actin polymerization status can trigger cell death (for review, see Franklin-Tong and Gourlay, 2008; Smertenko and Franklin-Tong, 2011) these cells may have ceased to regulate their ABP decoration, so that the Lifeact–psRFP binding motif became freely accessible.

The observed complete decoration of AF in transiently transformed BY-2 cells can be explained in a similar way. In a transient transformation, only cells with the highest level of expression are detected. Those cells are not viable over longer time periods, but are extremely stressed due to functional disruption of the cytoskeleton as a consequence of overexpression. In a stable transformation, only those cells will survive for which the expression of the probe does not impair cellular functions leading to natural selection of physiological levels of the probe.

To test whether Lifeact–psRFP overexpression affects the dynamics of AF, the transgenic BY-2 cell line was investigated with respect to Latrunculin B (LatB), a drug which binds and irreversibly sequesters G-actin, eliminating AF depending on their innate turnover. Stable actin bundles require a longer inhibitor exposure or higher concentration, dynamic AF are rapidly eliminated (Coué et al., 1987). Therefore, LatB sensitivity can be used to monitor AF stability. If the expression of Lifeact–psRFP would have increased the stability of AF *per se*, the cell culture should be less sensitive to LatB. However, the Lifeact–psRFP expressing cell line was clearly more sensitive (Fig. 4b), which argues against reduced dynamics of AF.

The nuclear actin basket — a spatial memory of cell polarity

Although the Lifeact–psRFP signal around the nucleus persisted, the spatial pattern varied during the cell cycle (Fig. 3). A clear cell cycle-dependent gradient was evident. In BY-2 cells, such a gradient was detected at the onset of mitosis, when the nucleus had completed migration to the cell center. There, the psRFP-labeled AF basket was very homogeneous and formed a tight meshwork around the nucleus. In contrast, nuclei still moving toward the cell center in preparation of mitosis showed a clear signal gradient toward their direction of migration. During mitosis, the labeled AF moved to the poles of the new daughter nuclei and subsequently formed a homogeneous meshwork around the nuclei (Fig. 2). After cytokinesis, the Lifeact–psRFP signal was exclusively found between the new cell wall and the daughter nuclei. It was possible to observe rotation of entire nuclei without re-orientation of the labeled AF, and how these nuclei were pulled into the new center of the cell. The signal of the nuclear basket was observed to be most intense at the anchor points of transvacuolar cytoplasmic strands that are maintained by AF and microtubules (Supplementary Data S3). These observations provide clear evidence that the labeled AF are actively regulated by the cell.

This observed link between perinuclear actin and nuclear movement raises questions about the underlying mechanisms and functions of this regulation. Principally, the unmasking of actin, as detected by the psRFP tetramer, might act either as a kind of intracellular signal or, alternatively, might define the competence of AF for actin-regulating signals. The impact of binding proteins or complexes for this signaling is conceivable. However, without any doubt, the labeled actin basket was characterized by a clearly visible stability. The nuclear basket and its polarity could probably function as a spatial memory for cell polarity. The question as to how cell polarity is inherited from the mother to the daughter cell, how the cytoskeleton can store and convey this directionality during cell division, and how nuclear position and migration affect this process are of utmost importance, but only poorly understood. Axis and polarity of cell growth and the reestablishment of cell polarity after cell division must be organized by still unidentified signals. The stability and orientation of the nuclear basket observed in Lifeact–psRFP expressing BY-2 cells could participate in this re-formation of cell polarity.

The LatB experiments could not detect reduced actin dynamics in the Lifeact–psRFP line (Fig. 4b). However, every visualization method is expected to alter and impair the marked system, however subtle this effect may be. In fact, our phenotyping data showed a slightly delayed nuclear migration compared to the non-transformed BY-2 WT shortly before mitosis (Fig. 4a). A similar effect was described by Frey et al. (2010) for BY-2 cells, in which a kinesin with the calponin-homology domain (KCH) from *Oryza sativa* had been overexpressed. AF, microtubules and KCH seem to cooperate in premitotic nuclear migration (Frey, 2011; Klotz and Nick, 2012). Participation of the Lifeact–psRFP-labeled actin basket in nuclear migration is consistent with the nuclear pulling model worked out for KCHs (Frey et al., 2010; Klotz and Nick, 2012).

If the stability and orientation of the nuclear basket observed in Lifeact–psRFP expressing BY-2 cells plays a pivotal role in the establishment of cell polarity in cells after mitosis, the basket should be a kind of starting scaffold for cytoskeletal re-formation. Therefore, Lifeact–psRFP expressing cells were protoplasted to mimick the loss of polarity following mitosis. Protoplasting transferred the BY-2 cells into a non-polar state, in which the cytoskeleton lacks any directional preference. After re-organization of the cytoskeleton in combination with nuclear movement, polarity develops newly in the cell providing the direction of growth. The persistence of the nuclear basket during this *tabula rasa* state (Supplementary Data S7), and its clear gradient during the cell cycle (Fig. 3), stimulates a model where the nucleus itself, or rather its actin basket, already harbors a basic polarity. This polarity could then be passed on to the daughter cells and trigger the establishment of cell polarity.

Super-resolution microscopy in living plant cells using photoactivation localization microscopy (PALM)

In animal cells, super-resolution microscopy already contributed to significant progress in the comprehension of the cytoskeleton. Plant cells, with their distinct three-dimensional structure stabilized by a rigid cell wall, pose additional challenges to fluorescence imaging as compared to the flat, adhering animal cells. The usage of pa-FPs instead of classical FPs, we were able to perform super-resolution microscopy in living plant cells with intact cell walls (Fig. 5).

This work not only demonstrates the feasibility of a stably expressed Lifeact–psRFP fusion for PALM imaging in plant cells, but also the possibility to reconstruct three-dimensional images from several super-resolved planes generated by analyzing thousands of individual CCD camera frames (Fig. 6). This technique, however, requires an excellent photostability of the employed pa-FP and slow dynamics of perinuclear actin so that image acquisition can keep up with the movements. Usually, PALM is applied to single sections within a sample due to photobleaching of the fluorophores below and above the focal plane when using wide-field illumination. Selective activation in the focal plane is possible using two-photon photoactivation (Fölling et al., 2007; Vaziri et al., 2008), yet this procedure requires high spatial and temporal photon densities and complicates microscope design. In the current work, we exploit the high stability of the perinuclear actin cage to combine the PALM approach with 3D sectioning (Fig. 5). This technique has great potential for cell biology, in particular, for plant cells. The live plant cell super-resolution PALM images presented here resolve cytoskeletal structures at a spatial scale of 20–50 nm, including lateral sectioning to obtain 3D models. By means of the Lifeact–psRFP fusion, we could visualize a lamellar arrangement of the perincuclear actin basket with AF that are wrapped around the nucleus.

These observations provoke and extend current models for nuclear migration in plant cells, where AF pull the nucleus (traction model, Fig. 8). The inevitable counterforce is supplied by cross-linking of AF to microtubules through KCHs (Frey et al., 2010; Klotz and Nick, 2012). This traction model requires that the nucleus is endowed with some kind of shape constancy. Nuclear lamins could not be demonstrated in plants, and plant analogs of the KASH-domain proteins that link nuclear envelope and cytoskeleton in animal cells have remained elusive. However, functional plant analogs of nuclear lamina proteins and lattice proteins for the envelope, so called SUN proteins are present (for review, see Boruc et al., 2012). Moreover, plant nuclei contain deep grooves and invaginations (Collings et al., 2000), such that a traction model is at least conceivable. However, the lamellar structure of the perinuclear actin basket, and the denser cables adjacent to the leading edge of nuclear migration as shown by our superresolution data favor an alternative view (bulging model, Fig. 8). These lamellar actin structures are clearly oriented parallel (and not perpendicular) to the surface of the nuclear envelope (see Supplementary Data S6). Contraction of the perinuclear actin lamella should constrict the adjacent region of the nuclear envelope such that it would bulge outwards, and the karyoplasm would be displaced into the newly arisen space. The counterforce for this contraction would again be mediated by cytoskeletal linkers tethering the lamella to the radial actin cables and microtubules.

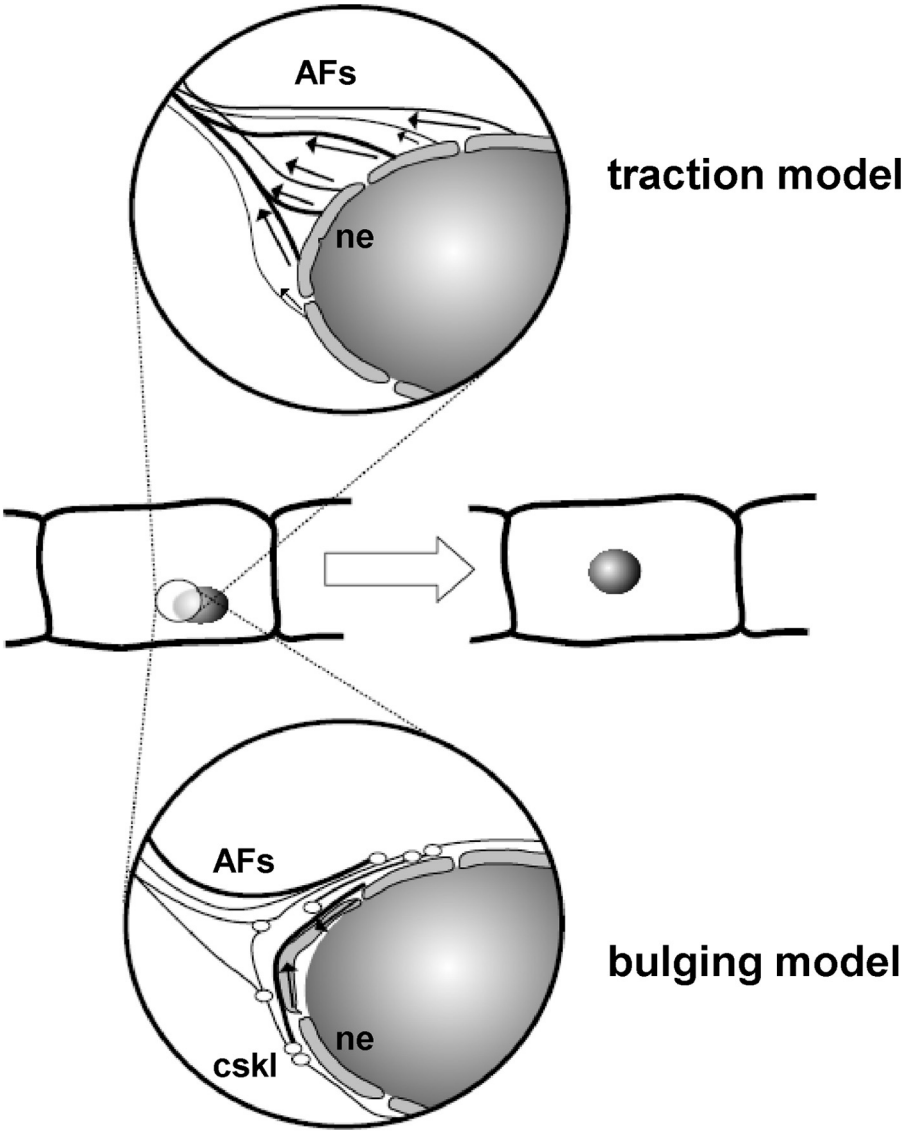

Fig. 8. Concurrent models for actin-driven nuclear migration. Traction model: radial actin cables (AFs) contract and pull the nucleus (arrows). Bulging model: lamellar actin cables contract (arrows) and cause a bulging of the nuclear envelope (ne). Since the lamellar cables are tethered to radial actin cables through cytoskeletal linkers (cskl), this will result in a displacement of the karyoplasm into the empty space provided by the bulge.

In the future, we will employ psRFP fused to Lifeact (or other proteins of interest) as a probe to address the problem of functional compartmentalization, *i.e.*, the coexistence of functionally distinct subsets of organelles or protein complexes without separation by a membrane.

Acknowledgments

This work was financially supported by the Deutsche Forschungsgemeinschaft, Center for Functional Nanostructures (CFN) projects E1.5 and E4.1. We thank A. Görnhardt, O. Huber and S. Purper for technical assistance. G.U.N. thanks Dr. J. Wiedenmann for a long-standing, fruitful collaboration.

Appendix A. Supplementary data

Supplementary data associated with this article can be found, in the online version, at http://dx.doi.org/10.1016/j.jplph.2013.10.007.

References

Betzig E, Patterson GH, Sougrat R, Lindwasser OW, Olenych S, Bonifacino JS, et al. Imaging intracellular fluorescent proteins at nanometer resolution. Science 2006;313:1642–5.
Boevink P, Oparka K, Santa Cruz S, Martin B, Betteridge A, Hawes C. Stacks on tracks: the plant Golgi apparatus traffics on an actin/ER network. Plant J 1998;15:441–7.
Boruc J, Zhou X, Meier I. Dynamics of the plant nuclear envelope and nuclear pore. Plant Physiol 2012;158:78–86.
Buschmann H, Green P, Sambade A, Doonan JH, Lloyd CW. Cytoskeletal dynamics in interphase, mitosis and cytokinesis analysed through Agrobacterium-mediated transient transformation of tobacco BY-2 cells. New Phytol 2011;190:258–67.
Collings DA, Carter CN, Rink JC, Scott AC, Wyatt SE, Allen NS. Plant nuclei can contain extensive grooves and invaginations. Plant Cell 2000;12:2425–39.
Coué M, Brenner SL, Spector I, Korn ED. Inhibition of actin polymerization by latrunculin A. FEBS Lett 1987;213:316–8.
Fölling J, Belov V, Kunetsky R, Medda R, Schönle A, Egner A, et al. Photochromic rhodamines provide nanoscopy with optical sectioning. Angew Chem Int Ed 2007;46:6266–70.
Franklin-Tong VE, Gourlay CW. A role for actin in regulating apoptosis/programmed cell death: evidence spanning yeast, plants and animals. Biochem J 2008;413:389–404.
Frey N, Klotz J, Nick P. A kinesin with calponin-homology domain is involved in premitotic nuclear migration. J Exp Bot 2010;61:3423–37.
Frey N. Dynamic bridges — an unconventional rice kinesin links actin and microtubules. Karlsruhe, Germany: Karlsruhe Institute of Technology; 2011 [PhD thesis].

Fuchs J. Characterization and application of photoswitchable fluorescent proteins for nanoscopy. Karlsruhe, Germany: Karlsruhe Institute of Technology; 2011 [PhD thesis].
Fuchs J, Böhme S, Oswald F, Hedde PN, Krause M, Wiedenmann J, et al. A photoactivatable marker protein for pulse-chase imaging with superresolution. Nat Methods 2010;7:627–30.
Hedde PN, Fuchs J, Oswald F, Wiedenmann J, Nienhaus GU. Online image analysis for photoactivation localization microscopy. Nat Methods 2009;6:689–90.
Hedde PN, Nienhaus GU. Optical imaging of nanoscale cellular structures. Biophys Rev 2010;2:147–58.
Hohenberger P, Eing C, Straessner R, Durst S, Frey W, Nick P. Plant actin controls membrane permeability. Biochim Biophys Acta 2011;1808:2304–12.
Hussey PJ, Allwood EG, Smertenko AP. Actin-binding proteins in the Arabidopsis genome database: properties of functionally distinct plant actin-depolymerizing factors/cofilins. Philos Trans R Soc Lond B Biol Sci 2002;357:791–8.
Kadota A, Yamadaa N, Suetsugub N, Hiroseb M, Saitod S, Shodad K, et al. Short actin-based mechanism for light-directed chloroplast movement in Arabidopsis. Proc Natl Acad Sci USA 2009;106:13106–11.
Kakimoto T, Shibaoka H. Actin filaments and microtubules in the preprophase band and phragmoplast of tobacco cells. Protoplasma 1987;140:151–6.
Kandasamy MK, McKinney EC, Meagher RB. A single vegetative actin isovariant overexpressed under the control of multiple regulatory sequences is sufficient for normal Arabidopsis development. Plant Cell 2009;21:701–18.
Karimi M, Inze D, Depicker A. Gateway vectors for Agrobacterium-mediated plant transformation. Trends Plant Sci 2002;7:193–5.
Klotz J, Nick P. A novel actin-microtubule cross-linking kinesin, NtKCH, functions in cell expansion and division. New Phytol 2012;193:543–5.
Kuss-Wymer CL, Cyr RJ. Tobacco protoplasts differentiate into elongate cells without net microtubule depolymerization. Protoplasma 1992;168:64–72.
Leduc C, Padberg-Gehle K, Varga V, Helbing D, Diez S, Howard J. Molecular crowding creates traffic jams of kinesin motors on microtubules. Proc Natl Acad Sci USA 2012;109:6100–5.
Lukyanov KA, Chudakov DM, Lukyanov S, Verkhusha VV. Innovation: photoactivatable fluorescent proteins. Nat Rev Mol Cell Biol 2005;6:885–91.
Maisch J, Nick P. Actin is involved in auxin-dependent patterning. Plant Physiol 2007;143:1695–704.
Maisch J, Fišerova J, Fischer L, Nick P. Actin-related protein 3 labels actin-nucleating sites in tobacco BY-2 cells. J Exp Bot 2009;60:603–14.
Mathur J, Mathur N, Hülskamp M. Simultaneous visualization of peroxisomes and cytoskeletal elements reveals actin and not microtubule-based peroxisome motility in plants. Plant Physiol 2002;128:1031–45.
Meagher RB, McKinney EC, Kandasamy MK. Isovariant dynamics expand and buffer the responses of complex systems: the diverse plant actin gene family. Plant Cell 1999a;11:995–1006.
Meagher RB, McKinney EC, Vitale AV. The evolution of new structures: clues from plant cytoskeletal genes. Trends Genet 1999b;15:278–84.
Nagata T, Nemoto Y, Hasezawa S. Tobacco BY-2 cell line as the "Hela" cell in the cell biology of higher plants. Int Rev Cytol 1992;132:1–30.
Nick P. Probing the actin-auxin oscillator. Plant Signal Behav 2010;5:94–8.
Nienhaus GU, Nienhaus K, Hölzle A, Ivanchenko S, Renzi F, Oswald F, et al. Photoconvertible fluorescent protein EosFP: biophysical properties and cell biology applications. Photochem Photobiol 2006;82:351–8.
Olyslaegers G, Verbelen JP. Improved staining of F-actin and colocalization of mitochondria in plant cells. J Microsc Oxford 1998;192:73–7.
Qiao F, Chang X, Nick P. The cytoskeleton enhances gene expression in the response to the Harpin elicitor in grapevine. J Exp Bot 2010;61:4021–31.
Riedl J, Crevenna AH, Kessenbrock K, Yu JH, Neukirchen D, Bista M, et al. Lifeact: a versatile marker to visualize F-actin. Nat Methods 2008;5:605–7.
Rust MJ, Bates M, Zhuang X. Sub-diffraction-limit imaging by stochastic optical reconstruction microscopy (STORM). Nat Methods 2006;3:793–5.
Sheahan MB, Rose RJ, McCurdy DW. Actin-filament-dependent remodeling of the vacuole in cultured mesophyll protoplasts. Protoplasma 2007;230:141–52.
Shimmen T, Yokota E. Cytoplasmic streaming in plants. Curr Opin Cell Biol 2004;16:68–72.
Shimmen T. The sliding theory of cytoplasmic streaming: fifty years of progress. J Plant Res 2007;120:31–43.
Smertenko A, Franklin-Tong VE. Organisation and regulation of the cytoskeleton in plant programmed cell death. Cell Death Differ 2011;18:1263–70.
Staiger CJ, Yuan M, Valenta R, Shaw PJ, Warn RM, Lloyd CW. Microinjected profilin affects cytoplasmic streaming in plant cells by rapidly depolymerizing actin microfilaments. Curr Biol 1994;4:215–9.
Staiger CJ, Blanchoin L. Actin dynamics: old friends with new stories. Curr Opin Plant Biol 2006;9:554–62.
Staiger CJ, Poulter NS, Henty JL, Franklin-Tong VE, Blanchoin L. Regulation of actin dynamics by actin-binding proteins in pollen. J Exp Bot 2010;61:1969–86.
Ueda H, Yokota E, Kutsuna N, Shimada T, Tamura K, Shimmen T, et al. Myosin-dependent endoplasmic reticulum motility and F-actin organization in plant cells. Proc Natl Acad Sci USA 2010;107:6894–9.
Van der Honing HS, van Bezouwen LS, Emons AM, Ketelaar T. High expression of Lifeact in *Arabidopsis thaliana* reduces dynamic reorganization of actin filaments but does not affect plant development. Cytoskeleton 2011;68:578–87.
Van Gestel K, Kohler RH, Verbelen JP. Plant mitochondria move on F-actin, but their positioning in the cortical cytoplasm depends on both F-actin and microtubules. J Exp Bot 2002;53:659–67.
Vaziri A, Tang J, Shroff H, Shank CV. Multilayer three-dimensional super resolution imaging of thick biological samples. Proc Natl Acad Sci USA 2008;105:20221–6.
Verbelen JP, Tao W. Mobile arrays of vacuole ripples are common in plant cells. Plant Cell Rep 1998;17:917–20.
Wiedenmann J, Nienhaus GU. Live-cell imaging with EosFP and other photoactivatable marker proteins of the GFP family. Expert Rev Proteomics 2006;3:361–74.
Wymer CL, Wymer SA, Cosgrove DJ, Cyr RJ. Plant cell growth responds to external forces and the response requires intact microtubules. Plant Physiol 1996;110:425–30.
Zaban B, Maisch J, Nick P. Dynamic actin controls polarity induction de novo in protoplasts. J Integr Plant Biol 2013;55:142–59.